Precise excitation-inhibition balance controls gain and timing in hippocampus

Aanchal Bhatia[1], Sahil Moza[1], Upinder S. Bhalla[#]
National Centre for Biological Sciences, Tata Institute of Fundamental Research, Bellary Road, Bangalore 560065 India

[1]Equal contribution
[#] Corresponding author (bhalla@ncbs.res.in)

Abstract

Balanced excitation and inhibition contributes to clamping excitability, sparse coding, and dynamic range expansion in many brain circuits. However, it is unknown if the balancing mechanism operates at the level of networks, ensembles or individual projections. We optogenetically stimulated hippocampal CA3 neurons in hundreds of different combinations, and monitored CA1 neuron responses in mouse brain slices. We observed that all input combinations from CA3, from tens of synapses to the order of single synapses, elicited excitation followed by tightly proportional inhibition. CA1 neurons summed these complementary inputs and exhibited gain control in the form of subthreshold divisive normalization (SDN). Biophysically, SDN emerged because inhibitory onset advanced toward excitatory onset with increasing input strength. This led to saturating peak amplitude and faster peak time, resulting in shared input information coding between the two. Our results suggest that SDN may be a general gain and timing control mechanism in balanced feedforward networks.

Introduction

Excitation and Inhibition (E and I) are normally closely balanced throughout the brain(Anderson et al. 2000; Wehr & Zador 2003a). EI balance is defined as the invariance in ratio of excitatory and inhibitory inputs to a cell (Okun and Lampl, Scholarpedia). Clinically, imbalance of excitation and inhibition at the level of networks is linked with several pathologies, including epilepsy, autism spectrum disorders and schizophrenia(Yizhar et al. 2011). Computationally, individual neurons integrate incoming excitation and inhibition to perform subtraction, division, and normalization of inputs(Isaacson & Scanziani 2011; Silver 2010). This has functional consequences such as preventing runaway excitation, gain control(Chance et al. 2002), maximizing sensitivity to various stimuli, and attentional modulation(Reynolds & Heeger 2009).

Strong EI correlations have been seen in several brain regions in response to various stimuli, for instance, series of tones in auditory cortex(Wehr & Zador 2003b; Zhang et al. 2003; Zhou et al. 2014), whisker stimulation in somatosensory cortex(Wilent & Contreras 2005), during cortical up states in vitro(Shu et al. 2003) and in vivo(Haider et al. 2006), during gamma oscillations in vitro and in vivo(Atallah & Scanziani 2009), and during spontaneous activity(Okun & Lampl 2008). However, presynaptic origins of balance are not well understood. It remains to be established if this balance results from a single presynaptic population, summation of multiple presynaptic populations, or from complex temporal dynamics of multiple presynaptic layers.

In the context of temporal dynamics and presynaptic origin, two key classifications of EI balance have been theoretically explored: ‘loose’ vs. ‘tight’(Denève & Machens 2016) (in the time domain), and ‘global’ vs. ‘detailed’(Vogels & Abbott 2009) (in the domain of granularity of input combinations). Neurons in loosely balanced EI networks are balanced only on slow timescales (~100 ms), leading to chaotic dynamics and unreliable spike times(van Vreeswijk & Sompolinsky 1996; Denève & Machens 2016; Shadlen & Newsome 1998). Conversely, neurons in tightly balanced EI networks receive input balanced at fast (<10 ms) timescales, and have reproducible spike times, making them good temporal coders(Denève & Machens 2016).

In the domain of granularity of input, there is a distinction between global and detailed balance. Global balance implies that neurons exhibit EI balance on average (for example, responses averaged over sensory inputs), whereas detailed balance implies that all subsets of

input neurons elicit balanced responses(Vogels & Abbott 2009). Based on the latter, neurons can effectively gate several inputs by reporting I/E ratio imbalances on arbitrary subsets of inputs, constituting an instantaneous information channel(Kremkow et al. 2010; Vogels & Abbott 2009). When detailed balance is also temporally tight, it is referred to as precise balance(Hennequin et al. 2017).

In this study we address two key open questions in the field. First, are synaptic inputs evoked by subsets of a single presynaptic network balanced for excitation and inhibition at the postsynaptic neuron? And second how do excitation and inhibition integrate to encode and communicate information across the synapse? We addressed these questions *in vitro*, to isolate the hippocampal network from background activity and to precisely control the stimulus. We stimulated channelrhodopsin-2 (ChR2) expressing CA3 neurons with tens to hundreds of optical patterns, and measured responses in CA1. We found that all randomly chosen subsets of CA3 neurons showed tightly coupled excitatory and feedforward inhibitory inputs to CA1 cell, thus, for the first time demonstrating precise balance(Hennequin et al. 2017) in the brain. We further examined the arithmetic form of the integration performed by this tightly balanced feedforward inhibitory network. We found that integration of excitation and feedforward inhibition leads to divisive normalization at subthreshold potentials. Moreover, this novel gain control operation leads to encoding of input information in both amplitude and timing of the response.

Results

Patterned optical stimuli in CA3 elicit subthreshold responses in CA1

To provide a wide range of non-overlapping stimuli, we performed patterned optical stimulation at channelrhodopsin-2 (ChR2) expressing CA3 neurons in acute hippocampal slices. We used CA3-cre mice to achieve CA3-specific localization of ChR2 upon injection of a Lox-ChR2 virus (**Fig. 1a, methods**). We used a DMD projector to generate spatiotemporal stimulus patterns in the form of a grid of several 16um x 16um squares, each approximating the size of a CA3 soma(Ishizuka et al. 1995) (**Fig. 1d, Supplementary Fig. 1**). The stimulus grid was centered at the CA3 cell body layer, and extended to the dendritic layer (**Fig. 1a**). Each stimulus pattern consisted of 1 to 9 such randomly chosen grid squares, presented at an inter-stimulus interval of 3 seconds (**Fig. 1a, 1d**, **Methods**). Several such stimulus patterns with a given number of input squares were randomly chosen from the grid to constitute a stimulus set. A

stimulus epoch typically consisted of 3 successive repeats of a stimulus set. We first characterized how CA3 responded to the grid stimulation (**Fig. 1b,e,f,g**). We confirmed that CA3 neurons fired reliably with a <2ms jitter, calculated as the standard deviation of the time of first spike (**Fig. 1f**) (n= 9, inputs=55, median= 0.43 ms). No desensitization occurred within a stimulus epoch, with the probability of spiking within an epoch remaining constant between the 3 repeats (**Fig. 1g**) (n = 7, number of stimulus epochs = 24). Thus, we could stimulate CA3 with hundreds of distinct optical stimuli in each experiment.

Next, we recorded postsynaptic potentials (PSPs) evoked at patched CA1 neurons by optically stimulating CA3 cells (**Fig. 1c,h,i,j**). A wide range of stimulus positions in CA3 excited the CA1 neurons (**Fig. 1c**). Most stimuli elicited subthreshold responses. Action potentials occurred in only 0.98% of trials in which stimuli ranged from 1 to 9 squares (18,668 trials, from 38 cells). This helped rule out any significant contribution of CA1 feedback interneurons for all our experiments. Responses to the same stimulus were consistent (84.74% responses showed less than 0.5 variance by mean (695 responses, 3 repeats each, n = 28) (**Fig. 1i**). Notably, the distribution of all 1 square responses had a mode at 0.25 mV, which is close to previous reports of a 0.2 mV somatic response of single synapses in CA1 neurons(Magee & Cook 2000)(8845 responses, n = 38) (**Fig. 1j**).

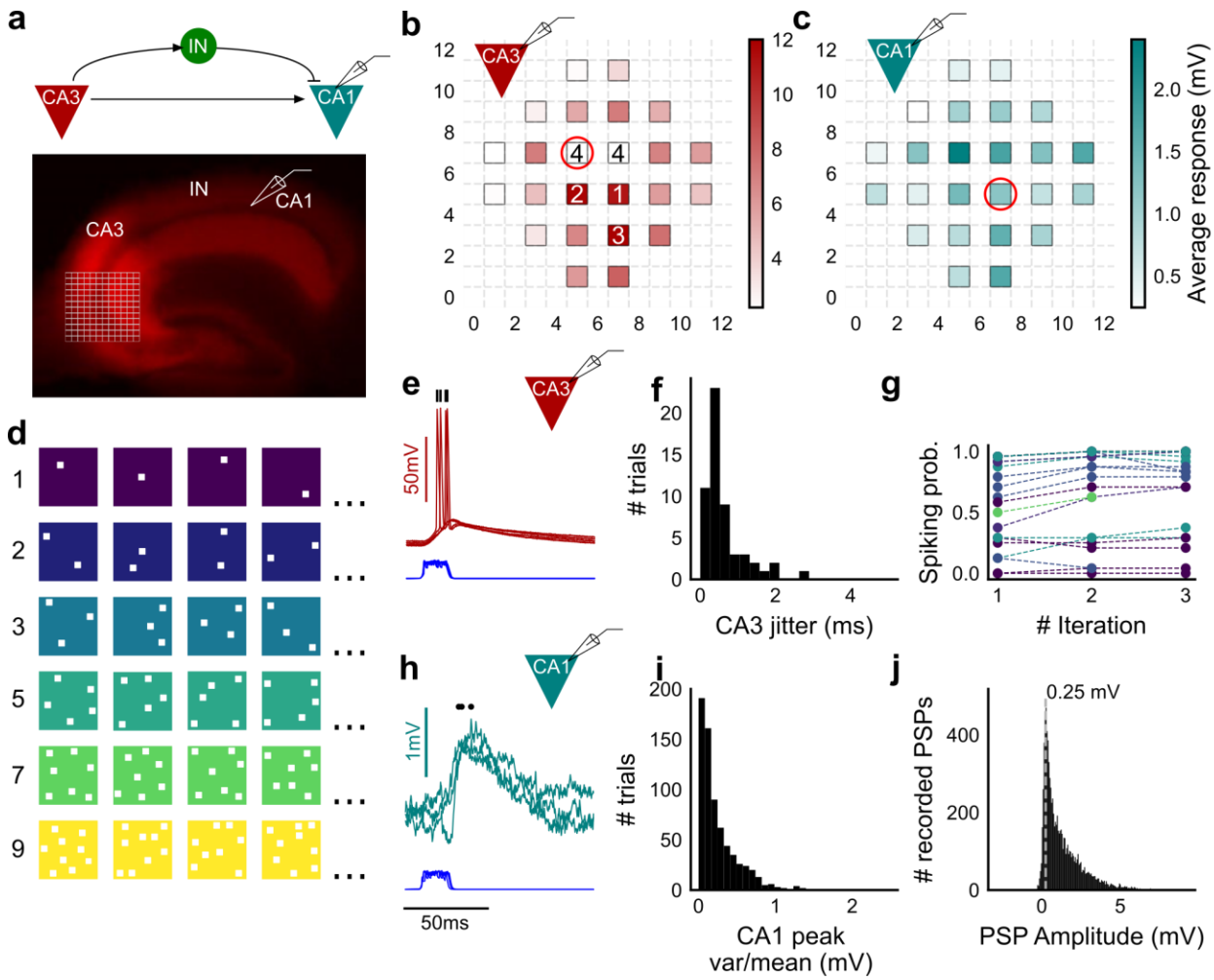

Figure 1: Patterned optical stimulation

(**a**) Top, schematic of the CA3-CA1 circuit with direct excitation and feed-forward inhibition from CA3 to CA1. Bottom, image of a hippocampus slice expressing ChR2-tdTomato (red) in CA3 in a Cre-dependent manner. In a typical experiment, the optical stimulation grid was centered at the CA3 cell body layer and CA1 neurons were patched.

(**b**) Heat map of CA3 neuron responses with 1 grid square active at a time. A CA3 neuron was patched and optically stimulated, in random temporal order, on the grid locations marked with a dark boundary. There were 24 such 1 square stimuli in the stimulus set. This cell spiked in response to 5 of the squares (with numbers inside), which were presumably closest to the cell body. Numbers in grid squares represent the count of trials (out of a total of 4 trials) in which a spike occurred. Color in grid squares represents peak subthreshold membrane potential change from baseline, averaged over trials when a spike did not occur.

(**c**) Heat map of CA1 responses while CA3 neurons were being stimulated by optical grid with 1 square active at a time. Colormap represents the peak subthreshold membrane potential, averaged over 3 repeats.

(**d**) Schematic of patterned optical stimuli used for stimulating CA3. Examples of input combinations of N-square stimuli (in columns), where N could be 1, 2, 3, 5, 7 or 9 (in rows).

(**e**) Spikes in response to 4 repeats for the square marked with a red circle, in **b**. Spike times are marked with a black tick, showing variability in peak times due to optical stimulation. Blue trace at the bottom marks the stimulus duration, as measured by a photodiode.

(**f**) Distribution of jitter in spike timing (SD) for all squares for all CA3 cells (n=9).

(**g**) Probability of spiking of all CA3 cells tracked over successive repeats within a stimulus epoch of a single recording session. Randomization of the stimulus pattern prevented desensitization of the ChR2 expressing cell. Probability was calculated as the fraction of times a spike happened for a given repeat of all stimuli presented within the epoch. Circles colored as in **d,** depict probability of a spike for one presentation of an N-square stimulus set (n = 7, epochs = 24). Connecting lines track the same input over 3 repeats.

(**h**) PSPs in response to 3 repeats for the square marked with a red circle in **c**. Peak times are marked with an asterisk. Blue trace at the bottom marks the stimulus duration, as measured by a photodiode.

(**i**) Distribution of peak PSP amplitude variability (variance/mean) for all squares for all cells. (n = 28, stimuli = 695)

(**j**) Histogram of peak amplitudes of all PSPs elicited by all 1-square stimuli, over all CA1 cells (n =38, trials = 8845). Gray dotted line represents the mode of the distribution.

Excitation and inhibition are tightly balanced for all arbitrarily chosen inputs to a cell

To examine the relationship between excitation and inhibition, we clamped CA1 neurons close to inhibitory (-70 mV) and excitatory (0 mV) reversal potentials. Restriction of ChR2 to CA3 pyramidal cells ensured that the recorded inhibition was purely feedforward and disynaptic. We first presented 5 different patterns of 5 squares each, at both of these potentials and recorded Excitatory and Inhibitory Post Synaptic Currents (EPSCs and IPSCs). We found strong proportionality between excitation and inhibition for every stimulus pattern (**Fig. 2a**). This suggested that even randomly chosen inputs from the CA3 may be balanced at CA1. Repetitions of the same pattern gave consistent responses, but different patterns gave different responses (**Fig. 2a**). This indicated that the optically-driven stimuli were able to reliably activate different subsets of synaptic inputs on the target neuron. Next, we asked, in what range of input strengths does random input yield balance? We presented 5 different patterns with 1, 2, 3, 5, 7 or 9 square combinations at both potentials. Surprisingly, all stimuli elicited proportional excitatory and inhibitory response, irrespective of response amplitude (**Fig. 2b, c**) (n =13, mean R^2 = 0.89+/- 0.06 SD). Given that the mode of single-square responses was ~0.25 mV, close to single synapse PSP estimates(Magee & Cook 2000) (**Fig. 1j**), we estimate that the granularity of the balance may be of the order of a single synapse. The slope of the regression line through all stimulus-averaged responses for a cell was used to calculate the Inhibition/Excitation (I/E) ratio for the cell. This proportionality factor was typically between 2 and 5 (**Fig. 2f**). The high R^2 values for all cells show tight proportionality for all stimuli (**Fig. 2g**). The proportionality and R^2 also remained roughly the same for increasing numbers of spots, again showing that they were not affected by the number of stimulus squares presented (**Fig. 2d,e**). Overall, we found a stimulus-invariant proportionality of excitation and inhibition for any randomly selected input, over a large stimulus range, suggesting that there is detailed balance(Vogels & Abbott 2009) in the CA3-CA1 circuit. Since balanced inhibition followed excitation at millisecond timescale, the CA3-CA1 feedforward circuit exhibited precise (both detailed and tight) balance(Hennequin et al. 2017).

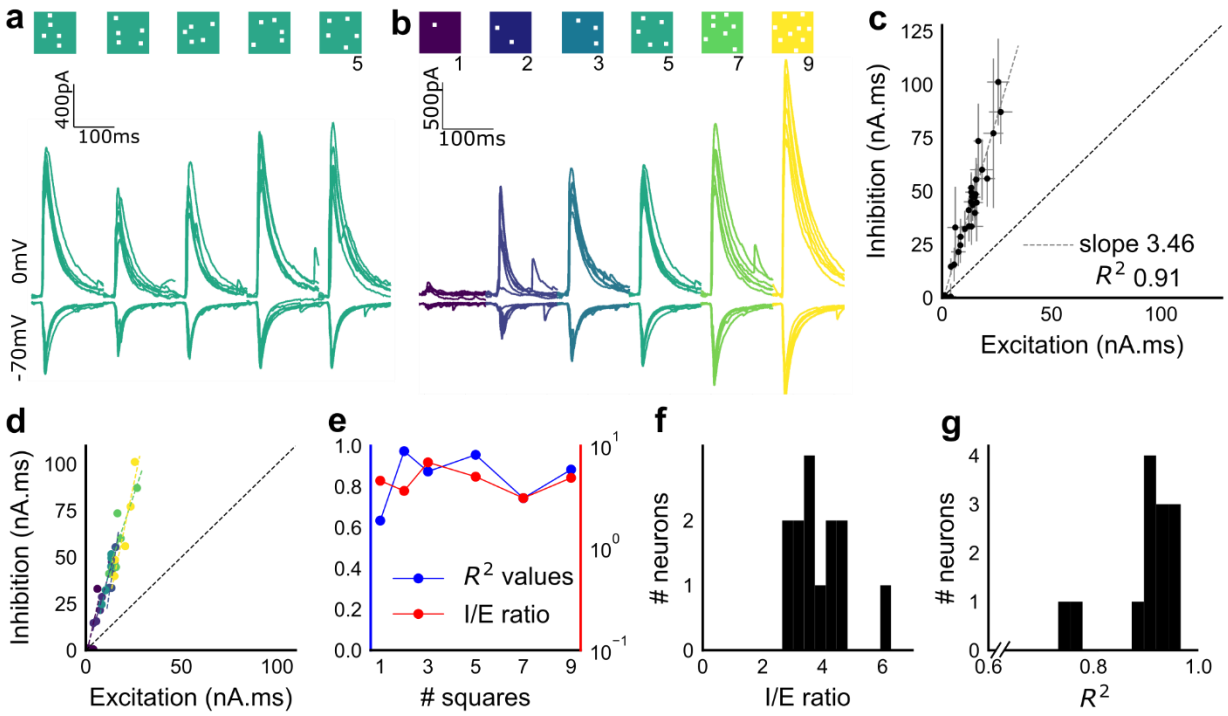

Figure 2: **Excitation and inhibition are tightly balanced for all stimuli**

(**a**) Monosynaptic excitatory postsynaptic currents (EPSCs, at 0mV) and disynaptic inhibitory postsynaptic currents (IPSCs, at -70mV) to 5 different stimulus combinations of 5 squares each. All combinations show proportional excitatory and inhibitory currents over 6 repeats. Top: schematic of 5 square stimuli.

(**b**) Proportional EPSCs and IPSCs in response to 6 repeats of 1 combination each, from 1 square to 9 square stimulus sets, for the same cell as in a. Top, schematic of the stimuli.

(**c**) Area under the curve for EPSC and IPSC responses, obtained by averaging over 6 repeats, plotted against each other for all stimuli to the cell in **a, b**. Error bars represent SD over repeats.

(**d,e**) Linear regression fits with quantification of I/E ratio and R^2 values for all combinations of 1, 2, 3, 5, 7 and 9 square stimulations, for the cell in **b**. Both I/E ratio and R^2 values remained consistent irrespective of number of squares.

(**f**) Summary of I/E ratio for all cells (n = 13).

(**g**) Summary for all cells of R^2 values of linear regression fits through all points. Note that 12 out of 13 cells had R^2 greater than 0.8, implying strong proportionality.

Combinatorial CA3-CA1 network inputs sum sublinearly

We next asked how these proportional excitatory and inhibitory inputs summed at CA1 neurons, close to resting potential. Based on anatomical studies, CA3 projections are likely to arrive in a distributed manner over a wide region of the dendritic tree of CA1 pyramidal neuron(Ishizuka et al. 1990)(**Fig. 3a**). While pairwise summation at CA1 has been shown to be largely linear in absence of inhibition(Cash & Yuste 1999), the degree of heterogeneity of summation in response to distributed excitatory and inhibitory synaptic inputs is not well understood(Gasparini 2006). To avoid biases that may arise from a single response measure during input integration(Poirazi et al. 2003), we examined PSPs using four different measures (**Fig. 3c**). These were peak amplitude, area under curve (AUC), average membrane potential and area under curve till peak (**Fig. 3c**).

We looked at input integration by presenting stimulus sets of 2, 3, 5, 7, or 9 input squares to a given cell, with each stimulus set ranging from 24 to 225 combinations of inputs. We also recorded the responses to all squares of the grid individually (1 square input). The observed response for a given square combination was plotted against the linear sum of responses of the individual squares constituting that combination (**Fig. 3b, d**). If the summation were perfectly linear, then a multi-square combination of inputs would elicit the same response as the sum of the responses to the individual squares (dotted line, **Fig. 3d**). **Figure 3e** shows responses of a single cell stimulated with 126 distinct 5-square combinations. The ‘observed’ response was sublinear as compared to the ‘expected’ summed response, for most stimuli (**Fig. 3e**). For all the four measures in **3c**, CA3 inputs summed sublinearly at CA1 (**Fig. 3e**). The sublinear summation suggested that inhibition divisively scales excitation, which was intuitive, given that excitation and inhibition were proportional for all stimuli. For all responses measured over all cells, 93.35% responses were individually sublinear, with distribution having mean 0.57± 0.31 (SD) **(Fig. 3f**). The slope of the regression line, which indicated the extent of sublinearity, varied between cells, with mean 0.38 ± 0.22 (SD) (n = 33) **(Fig. 3g**).

Thus, we found that the CA3-CA1 network exhibits sublinear summation over a large number of inputs.

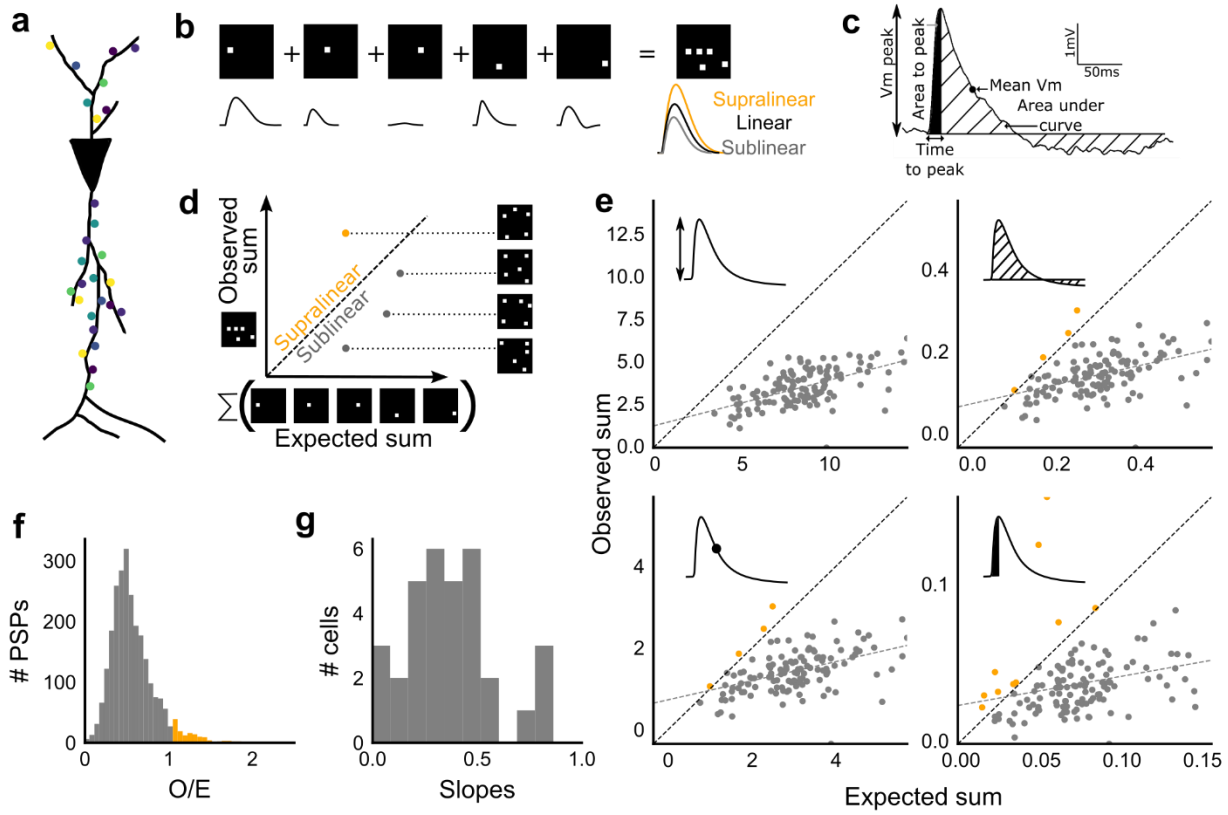

Figure 3: **CA3-CA1 network sums inputs sublinearly**

(**a**) Schematic of a neuron receiving synaptic input distributed over its dendritic tree.

(**b**) Schematic of input integration. Top, five 1-square stimuli presented individually, and a single 5-square stimulus comprising of the same squares. Bottom, PSPs elicited as a response to these stimuli. 5-square PSP can be larger (supralinear, orange), equal (linear, black), or smaller (sublinear, gray) than the sum of the single square PSPs.

(**c**) A PSP trace marked with the 5 measures used for further calculations. PSP peak, PSP area, area to peak, mean voltage and time to peak are indicated. The first 4 are used for the 4 plots in **e**.

(**d**) Schematic of the input integration plot. Each circle represents response to one stimulus combination. 'Observed' (true response of 5 square stimulation) on Y-axis and 'Expected' (linear sum of 1 square responses) is on X-axis.

(**e**) Most responses for a given cell show sublinear summation for a 5-square stimulus. The 4 panels show sublinear responses for 4 different measures (mentioned in **c**) for the same cell. The grey dotted line is the regression line and the slope of the line is the scaling factor for the responses for that cell. For peak (mV), area (mV.ms), average (mV), and area to peak (mV.ms); slope = 0.27, 0.23, 0.23, 0.18; R^2 0.57,

0.46, 0.46, 0.26 respectively. The responses to AUC and average are similar because of the similarity in the nature of the measure.

(**f**) Distribution of all responses for all 5-square stimuli (mean = 0.57, SD = 0.31), from all recorded cells pooled. 93.35% responses to 5-square stimuli were sublinear (2513 PSPs, n = 33).

(**g**) Distribution of slopes for 5-square stimuli (mean = 0.38, SD = 0.22). Regression lines for all cells show that all cells display sublinear (<1 slope) summation (n = 33).

CA3-CA1 network performs Subthreshold Divisive Normalization (SDN)

We then tested how the sublinearity scaled with a larger range of inputs. Inhibition has previously been shown to perform arithmetic operations like subtraction, division, and normalization(Carandini & Heeger 2012). We created a composite model to fit and test for three possibilities of E-I integration: subtractive inhibition, divisive inhibition, and divisive normalization (**Eqn. 1**). Here alpha (α) can be thought to be subtractive inhibition parameter, beta (β) as the divisive inhibition parameter, and gamma (γ) the normalization parameter (**Fig. 4a**).

$$O = E - \frac{\beta E}{\gamma + E} E - \alpha \qquad (\mathbf{1})$$

Using the framework of **Eqn. 1**, we asked what computation was performed at the CA3-CA1 network. We noted that nonlinear functions can be observed better with a large range of inputs(Poirazi et al. 2003) and therefore increased our stimulus range (**Supplementary Fig 5,6**). We presented many combinations of 2, 3, 5, 7 or 9 square stimuli to individual neurons (**Fig. 4b**). We selected cells with at least 50 input combinations, and pooled responses from all stimuli to a cell. Then, we fit equation 1 to them (**Fig. 4b**). From visual inspection, the subtractive inhibition model, $O = E - \alpha$ (fixing β, γ=0) was a bad fit, since intercepts (α) were close to 0 (**Fig. 4a**).

By fixing γ and α to 0 in **Eqn. 1,** we got Divisive Inhibition (DI) model:

$$O = E - \beta E \qquad (\mathbf{2})$$

Similarly, β was fixed to 1 and α to 0 to get Divisive Normalization (DN) model:

$$O = E - \frac{E}{\gamma + E} E \qquad (\mathbf{3})$$

In this form, decrease in γ implies increase in normalization (**Fig. 4a**). We used least-squares polynomial regression to fit DI and DN models to our data. The goodness of fit for all cells was tested by comparing BIC (Bayesian Information Criterion) (**Fig. 4c**) and reduced chi-squares of the models (**Supplementary Fig 7, Methods**). DN (α = 0, β = 1) was better than DI (α = 0, γ = 0) model in explaining the data (BIC: Two-tailed paired t-test, $P < 0.00005$, reduced chi-square: Two-tailed paired t-test, $P < 0.00005$, n = 32 cells).

The normalizing behavior can be clearly seen in **Figure 4b**, where the response evoked by 5 mV expected and 15 mV expected is very similar. Thus, evoked responses do not scale linearly with increasing inputs. This is how subthreshold divisive normalization can allow a large range of inputs to be integrated before reaching spike threshold. Thus we observed Subthreshold Divisive Normalization (SDN) as an outcome of integration of precisely balance in the CA3-CA1 network.

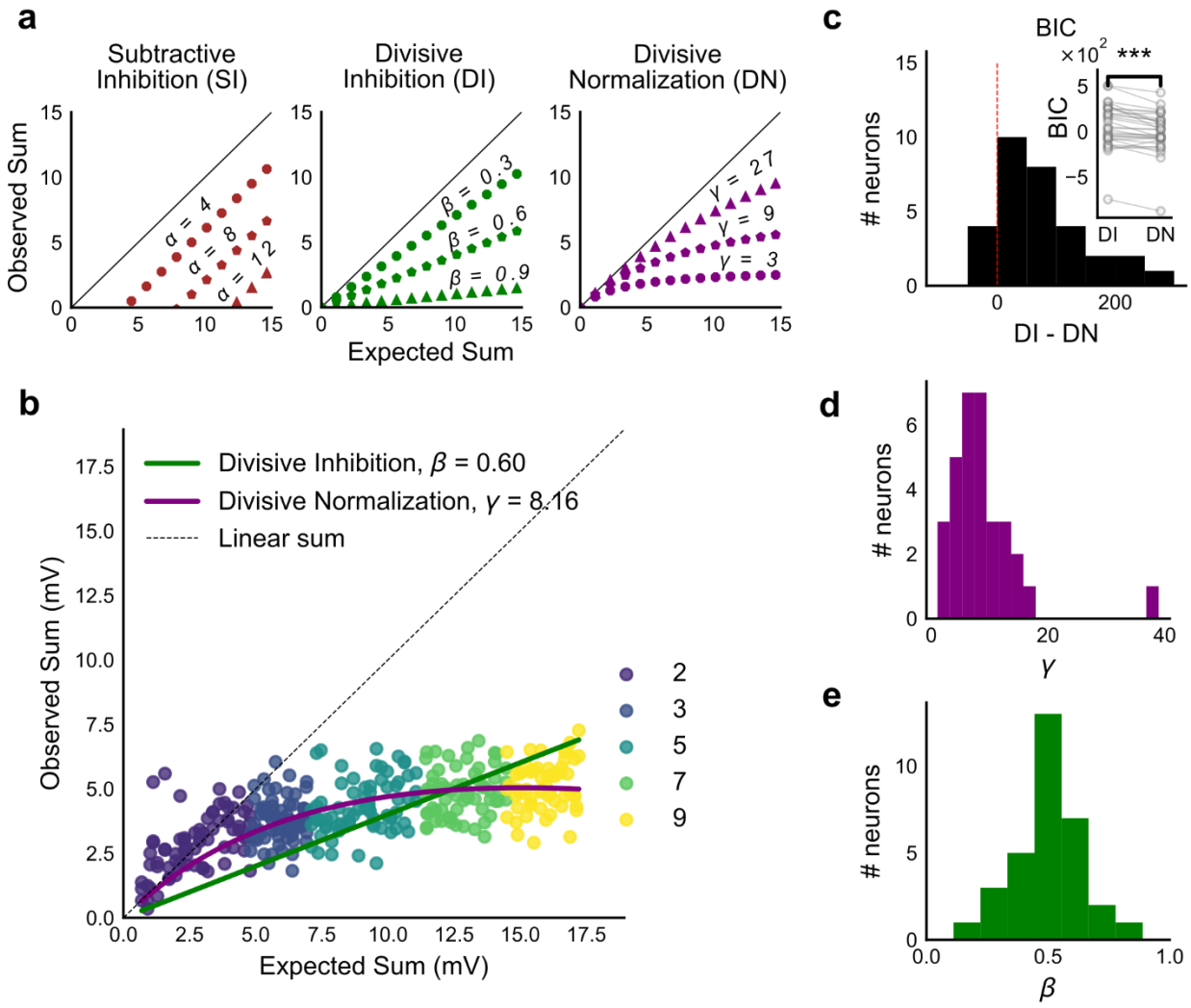

Figure 4: Subthreshold Divisive Normalization (SDN)

(**a**) Three models of how inhibition interacts with excitation and modulates membrane potential: (left to right) Subtractive Inhibition (SI), Divisive Inhibition (DI) and Divisive Normalization (DN).

(**b**) Divisive normalization seen in a cell stimulated with 1, 2, 3, 5, 7 and 9 square combinations. DN and DI model fits are shown in purple and green respectively.

(**c**) Difference in Bayesian Information Criterion (BIC) values for the 2 models - DI and DN. Most differences between BIC for DI and DN were less than 0, which implied that DN model fit better, accounting for the number of variables used. Insets show raw BIC values. Raw BIC values were consistently lower for DN model, indicating better fit (Two-tailed paired t-test, $P < 0.00005$).

(**d**) Distribution of the parameter γ of the DN fit for all cells (median = 7.9, n = 32).Compare with **a**, **b** to observe the extent of normalization.

(**e**) Distribution of the parameter beta of the DI fit for all cells (mean = 0.5, n = 32).Values are less than 1, indicating sublinear behaviour.

CA3 feedforward inhibition is necessary for subthreshold divisive normalization

We next tested our proposed inhibitory mechanism for the observed SDN by repeating the above experiment with inhibition blocked. We expected that SDN would be lost and linearity would be reinstated upon blocking inhibition.

We recorded from CA1 neurons with our array of optical stimuli (**Fig. 5a**), then applied GABAzine to the bath and repeated the stimulus array (**Fig. 5b**). We found that when inhibition was blocked, summation approached linearity (**Fig. 5b, c**). We compared the scaling parameter γ of the divisive normalization model fit, for the above two conditions. The values of γ were larger with inhibition blocked, indicative of approach to linearity (Wilcoxon rank-sum test, $P<0.05$, n = 8) (**Fig. 5c**). The cells with inhibition blocked showed residual sublinearity at high stimulus levels. Residual sublinearity in similar condition has been previously attributed to I_A conductance in CA1 neurons(Cash & Yuste 1999). Thus, we confirmed that blocking inhibition reduced sublinearity, attenuating SDN.

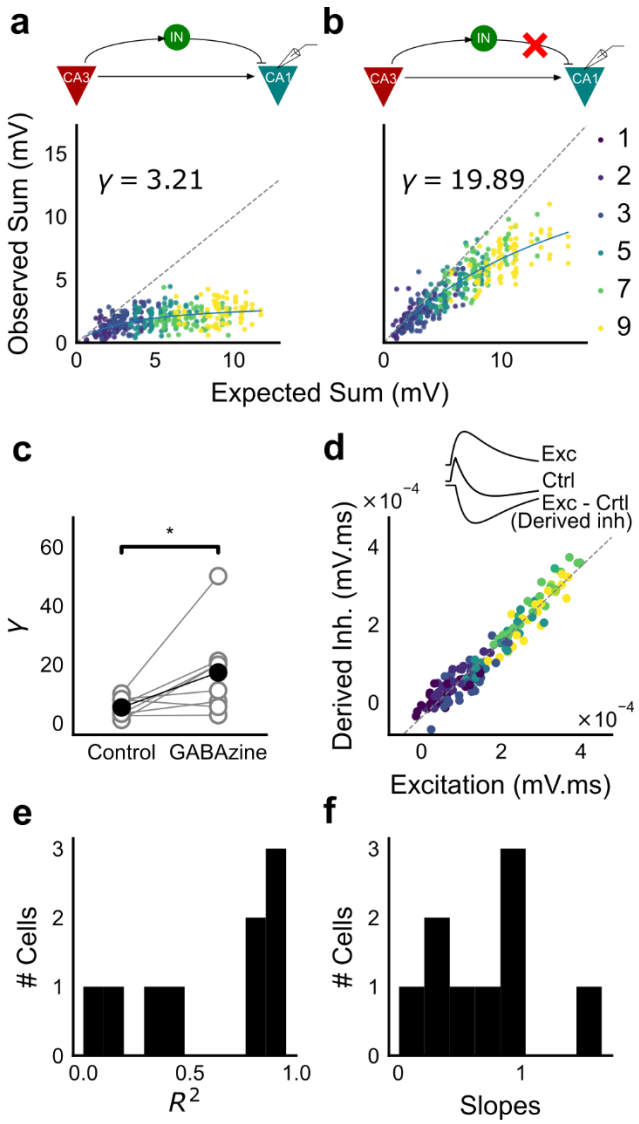

Figure 5: Inhibition is necessary for subthreshold divisive normalization

(**a**) Top, schematic of experiment condition. Bottom, a cell showing divisive normalization in control condition.

(**b**) Top, schematic of experiment condition with feedforward inhibition blocked (2uM GABAzine). Bottom, responses of the same cell with inhibition blocked. The responses are much closer to the linear summation line (dashed). The blue lines in **a**, **b** are the fits of the DN model. The value of γ of the fit increases when inhibition is blocked.

(**c**) The γ of the DN fits were calculated for both control and GABAzine case (n = 8). Most of them had larger γ with GABAzine in bath (Wilcoxon rank sum test, $P<0.05$, n = 8), implying lower normalization.

(**d**) Excitation versus derived inhibition for all points for the cell shown in **a** (area under the curve) (Slope = 0.97, r-square = 0.93, x-intercept = 3.75e-5 mV.ms). Proportionality was seen for all responses at resting membrane potential. 'Derived inhibition' was calculated by subtracting control PSP from the excitatory (GABAzine) PSP for each stimulus combination.
(**e,f**) R^2 (median = 0.8) and slope values (median = 0.7) for all cells (n = 8), showing tight EI proportionality, and slightly more excitation than inhibition at resting membrane potentials.

Detailed balance is also seen at resting membrane potential

We next compared responses to identical patterns before and after GABAzine application. For a given cell, for each pattern, we subtracted the initial control response from the corresponding response in presence of GABAzine. This gave us the inhibitory component or 'derived inhibition' for each stimulus pattern (**Fig. 5d, inset**). We found that all stimuli to a cell evoked proportional excitation and inhibition even when recorded at resting potential (**Fig. 5d**). Over the population, the median slope of the proportionality line was around 0.7, indicating that the EI balance was slightly tilted towards higher excitation than inhibition (**Fig 5f**). Overall, we saw detailed balance in evoked excitatory and inhibitory synaptic potentials for >100 combinations per neuron.

Inhibitory onset delay links tight balance, divisive normalization, and response timing

We made a single compartment conductance model (**Fig. 6b, Eqn. 5**) to analyze the mechanism of SDN. We fit a function of difference of exponentials (**Methods**) to our voltage clamp data to extract the peak amplitudes and kinetics of excitation and inhibition currents (**Methods**, **Fig. 6a**). We used these and other parameters from literature (**Supplementary** Table 1), and constrained the model to have EI balance, i.e. have maximum excitatory (g_{exc}) and inhibitory conductance (g_{inh}) proportional to each other, with a given I/E ratio. To test for SDN, we simulated our model with I/E ratios ranging from 0-5, in the range of experimentally determined I/E ratios.

We observed that EI balance with constant EI delay is consistent with the divisive inhibition model (**Fig. 6c**). Divisive normalization implies progressively smaller changes in membrane voltage amplitude with increase in excitatory input. This would require a non-linear increase in inhibition with increase in excitation. However, this is contradictory to the

observation of balanced excitation and inhibition for every input. We surmised that without changing EI balance, SDN should result if the inhibitory onset delays were an inverse function of the excitation (**Fig. 6e**, **Eqn. 4**). Hence, we simulated the model with different values of inhibitory delay (δ_{inh}) as a function of the excitation.

$$\delta_{inh} = \delta_{min} + me^{-kg_{exc}} \quad (4)$$

Here δ_{min} is the minimum synaptic delay between excitation and inhibition, k sets the steepness of the delay change with excitation, and *m* determines the maximum synaptic delay. Here we kept δ_{min} = 2 ms, k = 2 /nS, and m = 13 ms (**Fig 6e**).In **Fig. 6d**, we show that SDN emerged when we incorporated delays changing as a function of the total excitatory input to the model neuron.

We then tested this model prediction. From the EPSC and IPSC fits (**Methods**), we extracted excitatory and inhibitory onsets, and subtracted the average inhibitory onsets from average excitatory onsets to get delays (δ_{inh}) for each stimulus combination. We saw that δ_{inh} was indeed an inverse function of g_{exc} total excitation (**Fig. 6e, f**). Notably, the relationship of delay with conductance with data from all cells pooled, seems to be a single inverse function, and might be a network property (**Figure 6g**). Similar relationships between EI latency and strength have been seen in other brain regions(Heiss et al. 2008).This input dependent change in inhibitory delay could be attributed to quicker firing of interneurons with larger excitatory inputs. Apart from the variability due to release probability, some variance around the mean for delay in our dataset could be attributed to the jitter in CA3 response time due to optical stimulation. Thus with this mechanism, inhibition follows excitation in an input amplitude dependent manner at the millisecond timescale. Thus, inhibition clamps down the rising EPSP, resulting in saturation of PSP amplitude when excitation is increased (**Fig. 6d, 8**).

We then examined the sensitivity of SDN to proportionality, and delay between excitation and inhibition. To test if balance and predicted inhibitory delay relationship are required for SDN, we shuffled the balanced g_{inh} in relation withg_{exc}, and separately shuffled the relationship of δ_{inh} andg_{exc}. In both cases, SDN was strongly attenuated, implying that both EI balance and inverse scaling of inhibitory delay were necessary for SDN (**Fig. 6j, k**).

Thus our analysis of a conductance model suggests that SDN could be a general property of balanced feedforward networks, due to two characteristic features: EI balance and inhibitory kinetics. Each of these variables may be subject to modulation or network tuning to attain different amounts of normalization (**Fig. 6h**).

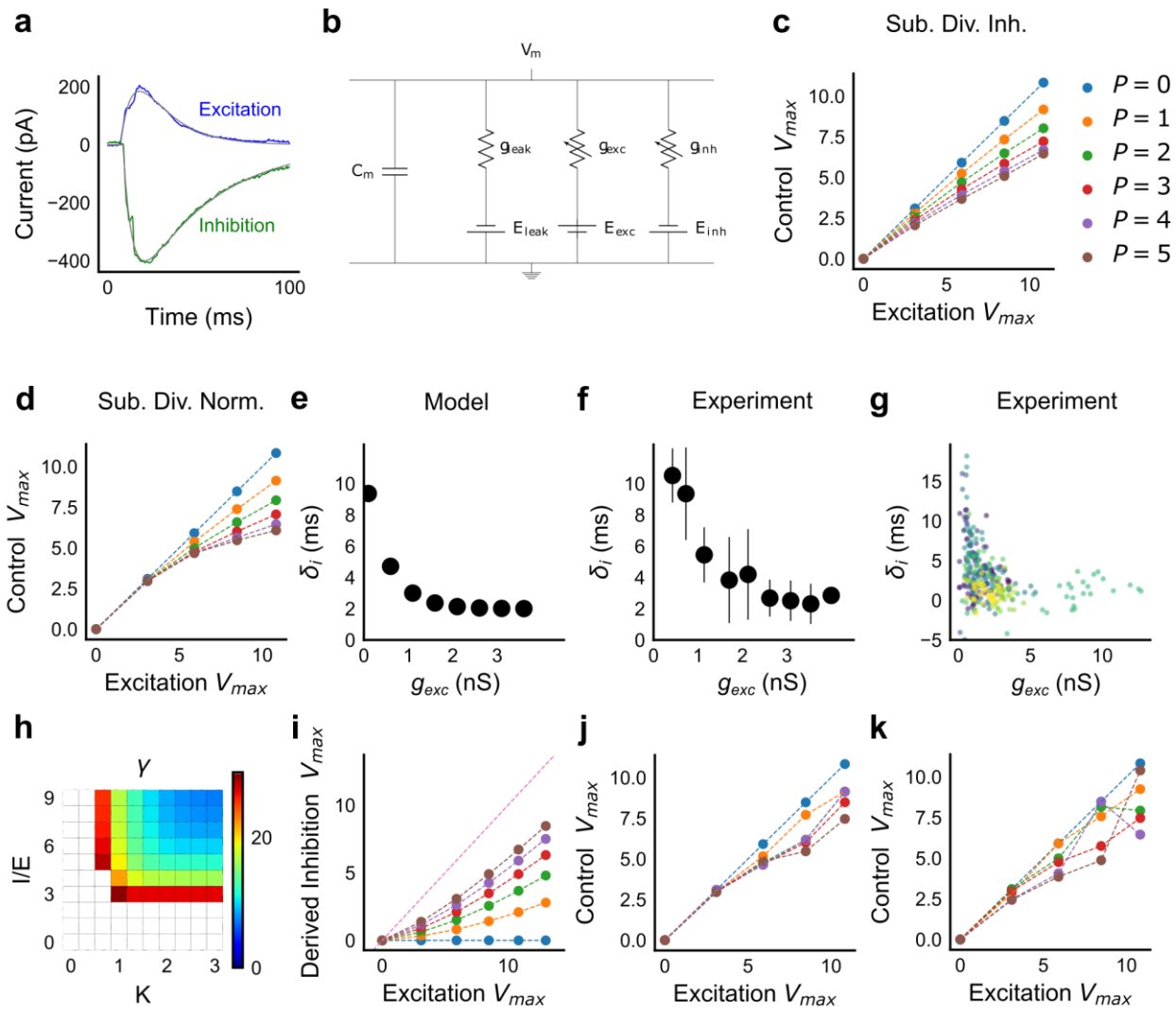

Figure 6: Conductance model predicts Excitatory-Inhibitory delay as an important parameter for divisive normalization.

(**a**) A difference of exponentials was fit to EPSC and IPSC traces to extract parameters to build a single compartment conductance model.

(**b**) Equivalent circuit for the conductance model showing capacitive, excitatory, inhibitory, and leak components.

(**c**) PSP peak amplitude with both excitatory and balanced inhibitory inputs is plotted against the EPSP peak amplitude with only excitatory input. Model showed divisive inhibition for I/E proportionality ranging from 0 to 5 when the inhibitory delay was kept constant. Different colours show I/E ratios (P).

(**d**) Same as in c, except the inhibitory delay was varied inversely with excitatory conductance (as shown in **e)**. Subthreshold Divisive Normalization (SDN) was observed, and the normalization gain was sensitive to the I/E ratio.

(**e**) Inverse relationship of E-I delays with excitation. Inhibitory delay was varied with excitatory conductance in **Eqn. 4**with δ_{min} = 2 ms, k = 2 /nS, and m = 13 ms.

(**f**) Data from an example cell showing the relationship of E-I delays with excitation. This is similar to the prediction in **e**.

(**g**) Data from all cells showing delay as a function of excitation. Different colours indicate different cells (n = 13).

(**h**) Heatmap of the Divisive normalization parameter (γ) as a function of I/E ratio and inhibitory delay kinetics (k), as predicted by the model. Changing I/E ratio or the rate of decline of the inhibitory delay affected the normalization gain.

(**i**) Excitation vs. derived inhibition shows a linear relationship. Derived inhibition was calculated by subtracting the PSP with no inhibition from PSP due to sum of excitation and inhibition (sameas**5d**). Different colors show different I/E ratio.

(**j,k**) Divisive normalization is sensitive to I/E ratio (**j**), and inhibitory delay δ_{min} (**k**). SDN is lost when the relationship between g_{exc} and g_{inh} is permuted or relationship between δ_{min} and g_{exc} is permuted.

Stimulus information is encoded both in amplitude and time

What does SDN mean for information transmission in balanced networks? While SDN allowed the cell to integrate a large range of inputs before reaching spiking threshold, it also resulted in saturation of PSP peaks at larger inputs (**Fig. 4c**). This implied that information about the input was partially 'lost' from the PSP amplitude. However, we observed that due to the decreasing EI delay (δ_{inh}) with increasing excitation (g_{exc}) (**Fig. 6e**), PSP times to peak became shorter, preserving some information about the input in time (**Fig 7a, c, Fig. 8**). In contrast, while the peak amplitudes seen with GABAzine predicted the input more reliably, peak times of EPSPs did not change much with input (**Fig. 7b,d**). Thus, PSP peak time may carry additional information about stimulus strength, when EI balance is maintained.

We quantified this using an information theoretical framework(Shannon 1948).We took linear sum of peak PSP amplitudes due to 1 square input (Expected sum), as a proxy for the input strength. We then calculated the mutual information between Expected sum and peak PSP amplitudes due to the corresponding N-squares, and between Expected sum and PSP peak timing (**Methods**). Using this, we asked, how is the information about the input divided between PSP peak amplitude and timing? We found that peak timing had more information when inhibition was present than when it was blocked (GABAzine), and peak amplitude had more information when inhibition was blocked (**Fig. 7f**). The total mutual information of both peak amplitude and peak timing with expected sum was slightly lesser in the presence of inhibition (Control) than in its absence (GABAzine), but this difference was statistically not significant (**Fig. 7e**) (Wilcoxon Rank sum test (< 0.05), P = 0.4, n = 7).Further, we asked, how much new information is gained with the knowledge of peak timing, when the peak amplitude is already known? We found that in the presence of inhibition, peak amplitude carried only a part of the total information about the input, and further knowledge of peak time substantially increased the total information. In contrast, in the absence of inhibition, peak amplitude carried most of the information about input, and there was very little gain in information with the knowledge of peak times (**Fig. 7f**) (Wilcoxon Rank sum test (< 0.05), n = 7).

Overall, these results suggest that with inhibition intact, input information is shared between amplitude and time, and knowledge of peak time and amplitude together contains more information about input than either of them alone.

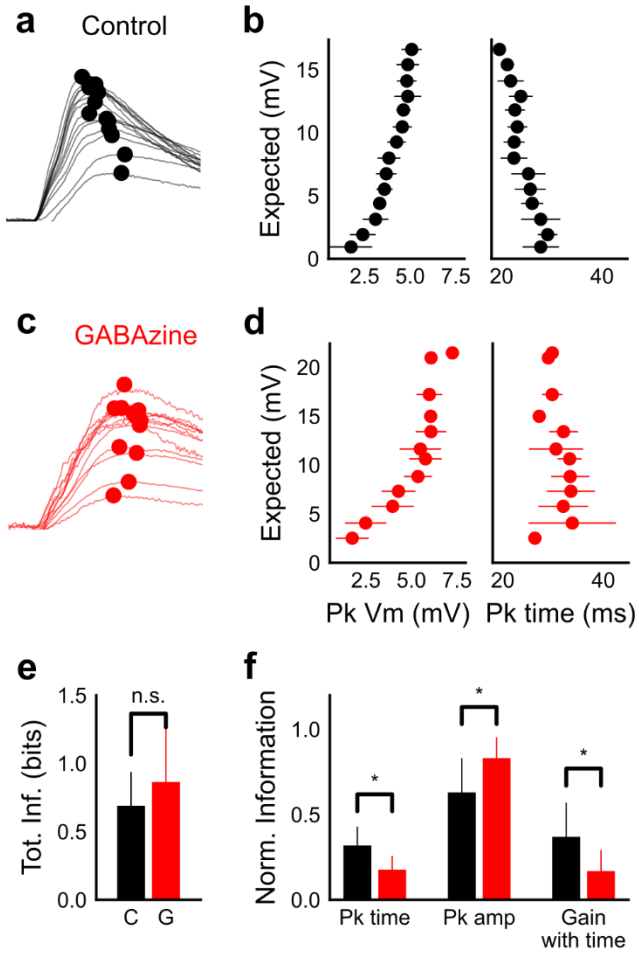

Figure 7: Input information is in PSP amplitude and time when both excitation and inhibition are present

(**a,c**) The peak arrives earlier as input gets larger in control case (black), but not with GABAzine in bath (red). Averaged traces for an example cell, control (black) and with GABAzine in bath (red). Each trace is averaged over all PSPs within a bin of 'expected sum' strength. Bin centres are as per y axis in panel c.

(**b**) Averaged peak Vm (PSP amplitude) and peak time plotted against Expected Vm. Both amplitude and time change as a function of input (Expected sum).

(**d**) Same as b, but in the presence of GABAzine. As a function of Expected sum, amplitude changes more than control, but time changes less than control.

(**e**) Total mutual information of peak amplitude and peak timing with expected sum is not significantly different between Control and GABAzine case (Wilcoxon Rank sum test (< 0.05), P = 0.4, n = 7).

(**f**) Normalized mutual information between Expected Vm and peak time, Expected Vm and peak amplitude, and conditional mutual information between Expected Vm and peak time, given the knowledge of peak amplitude. Normalized information was calculated by dividing mutual information by total information (**e**) for each cell. Black is control and red GABAzine (n = 7). Peak times carry more information in the presence of inhibition, and peak amplitudes carry more information in the absence of inhibition. There is higher gain in information about the input with timing if the inhibition is kept intact (Wilcoxon Rank sum test (< 0.05), n = 7)

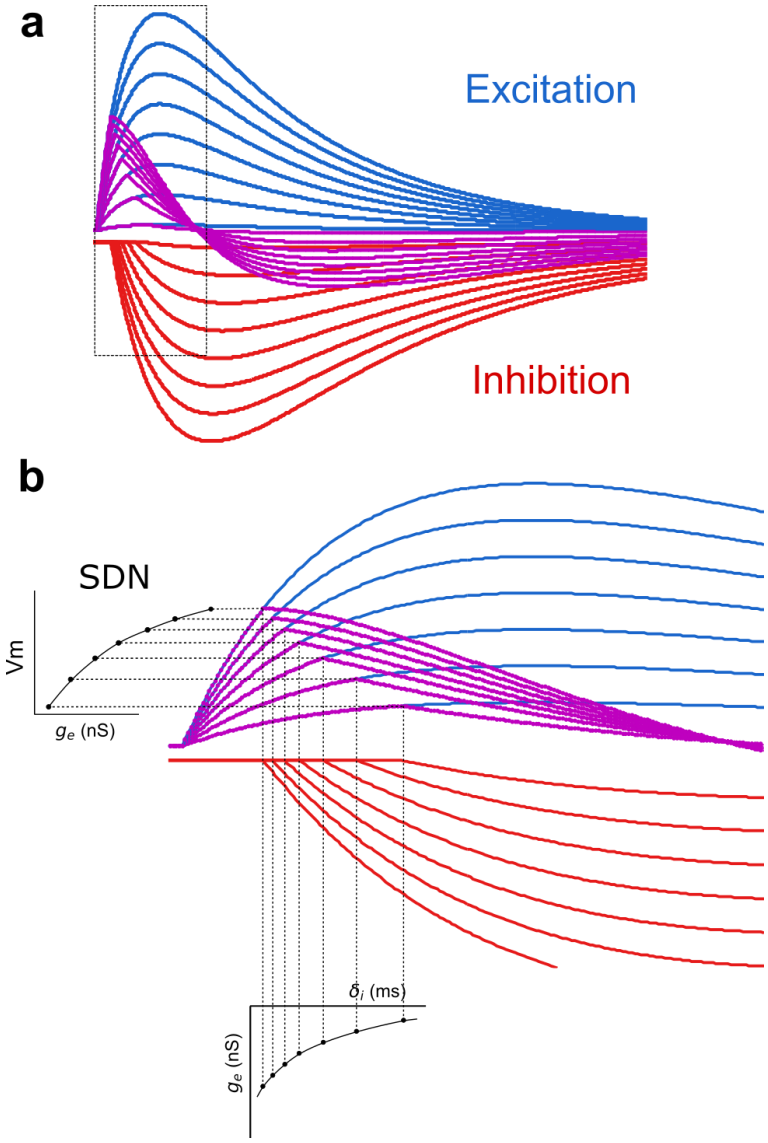

Figure 8: Schematic of how precisely balanced excitation and inhibition, coupled with dynamic EI delays, leads to SDN

(**a**) Schematic showing precisely balanced EPSPs (blue) and corresponding IPSPs (red) integrating to produce PSPs (purple). The EPSPs and IPSPs increase in equal input steps.

(**b**) Zooming into the portion in the rectangle in **a**. Excitation onset is constant, but inhibition onset changes as an inverse function of input or conductance (g_{exc}), as shown in **Figure 6e**. With increasing input, inhibition arrives earlier and cuts into excitation earlier for each input step. This results in smaller differences in excitatory peaks with each input step, resulting in SDN. The timing of PSP peaks (purple)

becomes progressively advanced, whereas the timing of EPSP peaks (blue) does not, consistent with our results in **Figure 7**.

Discussion

We have described biophysical features of a gain and timing control mechanism operating at individual neurons in precisely balanced feedforward circuits. We optically stimulated CA3 with a large number of stimulus combinations, and observed precise balance between excitation and inhibition at individual CA1 neurons for every input combination. Stronger stimuli from CA3 led to proportional increase in excitatory and inhibitory amplitudes at CA1, and a decrease in the delay with which inhibition arrived. Consequently, larger inputs led to progressively smaller changes in membrane potential, which we term subthreshold divisive normalization (SDN). SDN thus expands the dynamic range of individual neurons. This reduction in inhibitory delay with stronger inputs contributes to a division of input strength coding between PSP amplitude and PSP timing, and could be an important way of modulating CA1 spike-timing.

Precise balance in the hippocampus

We found that most arbitrary subsets of synaptic inputs from CA3 to a given CA1 neuron were balanced (**Fig. 2, 5d**) and inhibition followed excitation at millisecond timescales (**Fig 6f**). Using optogenetic, as opposed to electrical stimulation, we ensured that only CA3 pyramidal neurons were excited, and contributed to feedforward inhibition. Our findings demonstrate that EI balance is maintained by arbitrary combinations of neurons in the presynaptic network, despite the reduced nature of the slice preparation, with no intrinsic network dynamics. This reveals exceptional structure in the connectivity of the network. How this balance is attained remains to be shown, with the exception of the auditory cortex, where detailed balance has been shown to emerge using an inhibitory plasticity rule(Vogels et al. 2011; D'amour & Froemke 2015). Given that balance needs to be actively maintained(Xue et al. 2014; D'amour & Froemke 2015), we suspect that similar plasticity rules(Hennequin et al. 2017) might also exist in the hippocampus. Moreover, the change in inhibitory delay with increasing excitatory input may have interesting consequences for the inhibitory plasticity rule suggested theoretically(Vogels et al. 2011).

Subthreshold divisive normalization: a novel gain control mechanism

We propose a new form of gain control, which operates at the subthreshold level. Subthreshold divisive normalization (SDN) is a mechanism by which balanced neuronal networks control the gain of summation of synaptic input at single neuron level. SDN allows for the expansion of the dynamic range of inputs that a neuron can accommodate before reaching spike threshold. This is particularly useful for temporally coding, sparse spiking neurons like CA1(Ahmed & Mehta 2009). Our study was uniquely able to observe SDN because of the large range of inputs possible in our experiments. A narrow range of inputs, similar to what has been used earlier for pairwise summation experiments, is not well suited to characterizing summation nonlinearities, and this limitation has been pointed out by computational analyses(Poirazi et al. 2003).

So far, divisive normalization (DN) has only been observed for firing rates of neurons(Carandini & Heeger 2012). Moreover, while most experimental observations have been explained by the phenomenological divisive normalization equation, the mechanistic basis for normalization has been unclear. Our observations, made in the subthreshold regime, provide a clear biophysical model of how balanced excitatory and inhibitory synaptic inputs interact to produce divisive normalization. A major implication of SDN is that the gain of every input is normalized independently at synaptic (millisecond) timescales. As opposed to this, timescales of gain change in DN are averaged over longer periods, over which rates change.

Gain in firing rate based divisive normalization can be modulated by an independent ‘modulator channel’(Sherman & Guillery 1998) such as sensory background or background synaptic input(Carandini & Heeger 2012). In SDN, normalization would be entirely local to the affected synapses. Theoretically, altering the parameter γ changes the summation gain (**Eqn. 1**, **Fig. 4a**). γ can be controlled by the following two biophysical quantities: I/E ratio (**Fig. 6d,h** shows how the I/E ratio affects SDN); and the recruitment kinetics of the interneurons (k) (**Eqn. 2, Fig 6h**). I/E proportionality can be changed by neuromodulation(Froemke 2015; Froemke et al. 2007), by short term plasticity mechanisms(Klyachko et al. 2006; Bartley & Dobrunz 2015; Tsodyks & Markram 1997)or by disinhibition(Basu et al. 2016). Interneuron recruitment based changes have also been shown to exist in thalamocortical neurons(Gabernet et al. 2005). Thus, processes which independently change these quantities could in principle affect the dynamics of single neuron gain (**Fig 6h**).

A previous model of hippocampal gain control(Pouille et al. 2009) has suggested that CA1 input gain, unchanged at individual neurons, is controlled at the population level, by heterogeneous excitation and homogeneous inhibition. It implied that different cells differently reach spiking threshold because of different amounts of incoming EPSCs, even though the IPSCs were common between different cells. However, our results show that gain change occurs and can be modulated even at individual neurons in the subthreshold domain. Signals which modulate I/E proportionality and/or interneuron kinetics could modulate the gain of individual neurons, and also consequently the entire population. This two-step gain control implied that the dynamic range of the population may be higher than previously estimated.

The ability to alter the gain of individual neurons can be particularly relevant in case of place cell formation. CA1 cells can be categorized into silent and place cells, on the basis of reliable activity at specific spatial locations(Thompson & Best 1989). Previous work has shown higher subthreshold depolarization for place cells in novel environments than for silent cells(Epsztein et al. 2011; Cohen et al. 2017). Changing I/E ratio of a neuron could modulate its subthreshold depolarization, and could be a putative mechanism to convert silent to place cells.

Temporal coding and SDN

In several EI networks in the brain, inhibition is known to suppress excitation after a short time delay, leaving a “window of opportunity” for spiking to occur(Pouille & Scanziani 2001; Higley & Contreras 2006; Wehr & Zador 2003b). We have shown that balanced inhibitory input arrives with a delay modulated by the excitatory input. This helps encode the input information in both amplitude and timing of the PSP, thus partially decoupling spiking probability from spike timing. In other words, large inputs can be represented with fewer spikes, while conserving input information in spike timing, when naively it would seem that increasing the number of spikes might be the way to represent increasing input. Similar dual encoding has been observed in literature(Panzeri et al. 2001). Specifically, in CA1 cells, theta phase precession is a phenomenon wherein precise timing of the first spike within a theta cycle refines spatial information of place field greater than the firing rate alone(Jensen & Lisman 2000).

Notably, since SDN changes the “window of opportunity” in an excitation dependent manner, the neuron can transition from temporal integration mode at small input amplitudes to coincidence detection at large input amplitudes(Gabernet et al. 2005; Higley & Contreras 2006; Wehr & Zador 2003b). This dynamic regulation of the time window could also be relevant for

temporal gating of input signals(Kremkow et al. 2010; Bruno 2011). Mechanisms that alter I/E ratio or interneuron kinetics could in turn modulate the amplitude and timing gates independently. This temporal gating, combined with the amplitude gating by detailed balance(Vogels & Abbott 2009) could be a powerful mechanism for gating signals(Kremkow et al. 2010) in the hippocampus.

Gain modulation by SDN has two main requirements – precise balance and delay relationship (**Fig. 6e**). Given that feedforward precise balance may exist in the cortex, and delay change is simply a property of a feedforward networks, SDN might be a general mechanism of subthreshold gain control in cortical circuits. In conclusion, precise feedforward balance is an elegant circuit property that can control gain, timing and gating at individual neurons in neural circuits.

Methods

Animals

All experimental procedures were approved by the National Centre for Biological Sciences Institutional Animal Ethics Committee (Protocol number USB–19–1/2011), in accordance with the guidelines of the Government of India (animal facility CPCSEA registration number 109/1999/CPCSEA) and equivalent guidelines of the Society for Neuroscience. CA3-cre (C57BL/6-Tg (Grik4-cre) G32-4Stl/J mice, Stock number 006474) were obtained from Jackson Laboratories. The animals were housed in a temperature controlled environment with a 14-h light: 10h dark cycle, with *ad libitum* food and water.

Virus injections

21-30 days old male transgenic mice were injected with Lox-ChR2 (AAV5.CAGGS.Flex.ChR2-tdTomato.WPRE.SV40) virus obtained from University of Pennsylvania Vector Core. Injection coordinates used were -2.0mm RC, +/-1.9mm ML, -1.5mm DV. ~300-400nl solution was injected into the CA3 region with brief pressure pulses using Picospritzer-III (Parker-Hannifin, Cleveland, OH, USA). Animals were allowed to recover for at least 4 weeks following surgery.

Slice Preparation

8-16 week (4-8 weeks post virus injection) old mice were anesthetized with halothane and decapitated post cervical dislocation. Hippocampus was dissected out and 350um thick

transverse hippocampal slices were prepared. Slices (350 microns) were cut in ice-cold high sucrose ASCF containing (in mM) - 87 NaCl, 2.5 KCl, 1.25 NaH_2PO_4, 25 $NaHCO_3$, 75 sucrose, 10 glucose, 0.5 $CaCl_2$, 7 $MgCl_2$. For cut slice control experiments, CA3 was removed at this stage. Slices were stored in a holding chamber, in artificial cerebro-spinal fluid (aCSF) containing (in mM) - 124 NaCl, 2.7 KCl, 2 $CaCl_2$, 1.3 $MgCl_2$, 0.4 NaH_2PO_4, 26 $NaHCO_3$, and 10 glucose, saturated with 95% O_2/5% CO_2. After at least an hour of incubation, the slices were transferred to a recording chamber and perfused with aCSF at room temperature.

Electrophysiology

Whole cell recording pipettes of 2-5MO were pulled from thick-walled borosilicate glass on a P-97 Flaming/Brown micropipette puller (Sutter Instrument, Novato, CA). Pipettes were filled with internal solution containing (in mM) 130 K-gluconate, 5 NaCl, 10 HEPES, 1 EGTA, 2 $MgCl_2$, 2 Mg-ATP, 0.5 Na-GTP and 10 Phosphocreatinine, pH adjusted to 7.3, osmolarity ~285mOsm. The membrane potential of CA1 cells was maintained near -65mV, with current injection, if necessary. GABA-A currents were blocked with GABAzine (SR-95531, Sigma) at 2uM concentration for some experiments. Cells were excluded from analysis if the input resistance changed by more than 25% or if membrane voltage changed more than 2.5mV (maximum current injected to hold the cell at the same voltage was +/-15 pA) of the initial value. For voltage clamp recordings, the K-gluconate was replaced by equal concentration Cs-gluconate. Cells were voltage clamped at 0mV (close to calculated excitation reversal) and -70mV (calculated inhibition reversal) for IPSC and EPSC recordings respectively. At 0mV a small component of APV sensitive inward current was observed, and was not blocked during recordings. Cells were excluded if series resistance went above 25MO or if it changed more than 30% of the initial value, with mean series resistance being 15.7MO +/- 4.5MO std (n=13). For whole-cell recordings, neurons were visualized using infrared microscopy and differential interference contrast (DIC) optics on an upright Olympus BX61WI microscope (Olympus, Japan) fitted with a 40X (Olympus LUMPLFLN, 40XW), 0.8NA water immersion objective.

Data Acquisition

Recordings were acquired on a HEKA EPC10 double plus amplifier (HEKA Electronik, Germany) and filtered 2.9 kHz and digitized at 20 kHz. All analysis was done using custom written software in Python 2.7.12 and MatlabR2012b.

Optical stimulation setup

Optical stimulation was done using DMD (Digital Micromirror Device) based Optoma W316 projector (60Hz refresh rate) with its color wheel removed. Image from the projector was miniaturized using a Nikon 50mm f/1.4D lens and formed at the focal plane of the tube lens, confocal to the sample plane. The white light from the projector was filtered using a blue filter (Edmund Optics, 52532), reflected off of a dichroic mirror (Q495LP, Chroma), integrated into the light path of the Olympus microscope, and focused on sample through a 40X objective. This arrangement covered a circular field of around 200 micron diameter on sample. 2.5 pixels measured 1 micron at sample through the 40X objective. Light intensity, measured using a power meter, was about 150mW/mm^2 at sample surface. Background light from black screen usually elicited no or very little response at recorded CA1 cells. A shutter (NS15B, Uniblitz) was present in the optical path to prevent the slice from being stimulated by background light during the inter-trial interval. The shutter was used to deliver stimulus of 10-15ms per trial. A photodiode was placed in the optical path after the shutter to record timestamps of the delivered stimuli.

Patterned optical stimulation

Processing 2 was used for generating optical patterns. All stimuli were 16 micron squares sub sampled from a grid. 16 micron was chosen since it is close to the size of a CA3 soma. The light intensity and square size were standardized to elicit typically 1 spike per cell per stimulus. The number of spikes varied to some extent based on the expression of ChR2, which varied from cell to cell. A single trial consisted of a 10-15ms stimulus and inter-trial interval of3 sec. The switching of spots from one trial to next prevented desensitization of ChR2 over successive trials (**Fig. 1g**).

For a patched CA1 cell, the number of connected CA3 neurons stimulated per spot is estimated to be in the range of 1 to a maximum of 50 for responses ranging from 0 to 2mV. These calculations were done assuming a contribution of 0.2mV per synapse(Magee & Cook 2000) and release probability of ~0.2(Murthy et al. 1997). This number includes responses from passing axons, which could also get stimulated in our preparation.

We did not observe any significant cross stimulation of CA1 cells. CA1 cells were patched and the objective was shifted to the CA3 region of the slice, where the optical patterns were then projected. CA1s showed no response to optical stimulation because of (i) restriction

of ChR2 to CA3 cells, (ii) physical shifting of the objective away from CA1 also made sure that any leaky expression, if present, did not elicit responses.

We used the following stimulus grids: 24 square circular sparse grid (Figure 1) (16 cells), 112 point dense circular grid (4 cells), 13x13 dense grid (9 cells), 15x15 dense grid (10 cells). All squares from a grid were presented individually (in random order) and in a stimulus set - randomly chosen combinations of 2, 3, 5, 7, or 9, with 2 or 3 repeats of each combination. The order of presentation of a given N square combination was randomized from cell to cell.

Data Analysis:

Data analysis was done using Python, numpy, scipy, matplotlib and other free libraries. All analysis code is available as a free library at (https://github.com/sahilm89/linearity).

Pre-processing

PSPs and PSCs were filtered using a low pass Bessel filter at 2 kHz, and baseline normalized using 100 ms before the optical stimulation time as the baseline period. Period of interest was marked as 100 ms from the beginning of optical stimulation, as it was the typical timescales of PSPs. Timing of optical stimulation was determined using timestamp from a photodiode responding to the light from the projector. Trials were flagged if the PSP in the interest period were indistinguishable from baseline period due to high noise, using a 2 sample KS test (p-value < 0.05). Similarly, action potentials in the interest period were flagged and not analyzed, unless specifically mentioned.

Feature extraction

A total of 4 measures were used for analyzing PSPs and PSCs (**Fig. 3c**). These were mean, area under the curve, average and area to peak. This was done to be able to catch differences in integration at different timescales, as suggested by Poirazi et al.,(Poirazi et al. 2003). Trials from CA1 were mapped back to the grid locations of CA3 stimulation for comparison of Expected and Observed responses. Grid coordinate-wise features were calculated by averaging all trials for a given grid coordinate.

Subthreshold Divisive Normalization model

Different models of synaptic integration: Subtractive Inhibition, Divisive Inhibition, and Divisive Normalization models were obtained by constraining parameters in **Equation 1**. The

models were then fit to the current clamp dataset using lmfit. Reduced chi-squares (**Supplementary Fig 7**) and Bayesian Information Criterion (**Fig 4c**) were used to evaluate the goodness of fits of these models to experimental data.

Single compartment model

A single compartment conductance based model was created in Python using sympy and numpy. The model consisted of leak, excitatory and inhibitory synaptic conductances (**Eqn.5**, **Fig 6b**.) to model the subthreshold responses by the CA1 neurons.

$$C_m \frac{dV_m}{dt} = g_{leak}(V_m - E_{leak}) + g_{exc}(V_m - E_{exc}) + g_{inh}(V_m - E_{inh}) \quad \textbf{(5)}$$

The parameters used for the model were taken directly from data, or literature (Supplementary **Table1**). The synaptic conductances$g_{exc}(t)$, and $g_{inh}(t)$ were modeled as difference of exponentials (**Eqn. 6 and 7**):

$$g_{exc}(t) = \bar{g}_{exc} \left(\frac{e^{\left(\frac{-t}{\tau_{decay}}\right)} - e^{\left(\frac{-t}{\tau_{rise}}\right)}}{-\left(\frac{\tau_{rise}}{\tau_{decay}}\right)^{\frac{\tau_{decay}}{\tau_{decay} - \tau_{rise}}} + \left(\frac{\tau_{rise}}{\tau_{decay}}\right)^{\frac{\tau_{rise}}{\tau_{decay} - \tau_{rise}}}} \right) \quad \textbf{(6)}$$

$$g_{inh}(t) = \bar{g}_{inh} \left(\frac{e^{\left(\frac{\delta_{inh} - t}{\tau_{decay}}\right)} - e^{\left(\frac{\delta_{inh} - t}{\tau_{rise}}\right)}}{-\left(\frac{\tau_{rise}}{\tau_{decay}}\right)^{\frac{\tau_{decay}}{\tau_{decay} - \tau_{rise}}} + \left(\frac{\tau_{rise}}{\tau_{decay}}\right)^{\frac{\tau_{rise}}{\tau_{decay} - \tau_{rise}}}} \right) \quad \textbf{(7)}$$

For the divisive normalization case, the inhibitory delays (δ_{inh}) were modeled to be an inverse function of $g_{exc}(t)$ (**Eqn. 4**). In other cases, they were assumed to be constant and values were taken from **Supplementary Table 1**.

Fitting data

Voltage clamp data was fit to a difference of exponential functions (**Eqn.8, Supplementary Fig 9**) by a non-linear least squares minimization algorithm using lmfit, a freely

available curve fitting library for Python. Using this, we obtained amplitudes ($\overline{g}$), time course (τ_{rise},τ_{decay}) and onset delay from stimulus (δ_{onset}) for both excitatory and inhibitory currents. We then calculated inhibitory onset delay (δ_{inh}) by subtracting onset delayof excitatory from inhibitory traces.

$$g(t) = \overline{g}\left(\frac{e^{\left(\frac{\delta_{onset} - t}{\tau_{decay}}\right)} - e^{\left(\frac{\delta_{onset} - t}{\tau_{rise}}\right)}}{-\left(\frac{\tau_{rise}}{\tau_{decay}}\right)^{\frac{\tau_{decay}}{\tau_{decay} - \tau_{rise}}} + \left(\frac{\tau_{rise}}{\tau_{decay}}\right)^{\frac{\tau_{rise}}{\tau_{decay} - \tau_{rise}}}}\right) \quad \textbf{(8)}$$

Mutual Information calculation

Mutual information was calculated by the histogram method. The calculated linear sum from one square PSP peak amplitude responses, measured N-square peak amplitudes and time were binned with equal number of bins. The bins were calculated using Sturges' Rule. Bin frequencies were divided by the total number of responses to get the probability of occurrence $p(x)$ of each bin. Mutual Information was then calculated for all pairs of combinations between linear sum, peak amplitude and time using **Eqn. 9 and 10**.

$$MI(X,Y) = H(X) + H(Y) - H(X,Y) \quad \textbf{(9)}$$

Where Shannon's entropy$H(X)$ for a variable$X$, is given as:

$$H(X) = \sum_{x \in X} - p(x) \log_2 p(x) \quad \textbf{(10)}$$

Further, conditional mutual Information was calculated to measure gain in information about input (linear sum) by knowledge of peak timing when peak amplitude is already known. It was calculated using **Equation 11**.

$$I\,(X\,;Y|Z) = H\,(X,Z) + H(Y,Z) - H(X,Y,Z) - H(Z) \quad \textbf{(11)}$$

Normalized mutual information was calculated by dividing mutual information between pairs of variables by the total information between all three variables (**Equation 12**).

$$I\,(X;Y,Z) = H\,(Z) + H(X,Y) - H(X,Y,Z) \quad \textbf{(12)}$$

Acknowledgements

AB and SM were supported by NCBS/TIFR and Council of Scientific and Industrial Research (CSIR). We acknowledge support from the University Grants Commission/Israel Science Foundation grant (UGC/ISF No. F 6-18/2014(IC)). We acknowledge the National Mouse Resource (NaMoR) facility funded by Department of Biotechnology for housing and maintaining all animals used in this study. We would like to thank Nikhila Krishnan and Shriya Palchaudhuri for help with genotyping; and Kambadur Ananthamurthy, Sathyaa Sakthi, Deepanjanli Dwivedi, Oliver Muthmann, Aditya Gilra, Arvind Kumar and Rishikesh Narayanan for discussions and suggestions on the manuscript.

Ahmed, O.J. & Mehta, M.R., 2009. The hippocampal rate code: anatomy, physiology and theory. *Trends in Neurosciences*, 32(6), pp.329–338.

Anderson, J.S., Carandini, M. & Ferster, D., 2000. Orientation tuning of input conductance, excitation, and inhibition in cat primary visual cortex. *Journal of neurophysiology*, 84(2), pp.909–926.

Atallah, B. V & Scanziani, M., 2009. Instantaneous Modulation of Gamma Oscillation Frequency by Balancing Excitation with Inhibition. *Neuron*, 62(4), pp.566–577. Available at: http://dx.doi.org/10.1016/j.neuron.2009.04.027.

Bartley, A.F. & Dobrunz, L.E., 2015. Short-term plasticity regulates the excitation/inhibition ratio and the temporal window for spike integration in CA1 pyramidal cells. *European Journal of Neuroscience*, 41(February), pp.1402–1415.

Basu, J. et al., 2016. Gating of hippocampal activity, plasticity, and memory by entorhinal cortex long-range inhibition. *Science*, 351(6269), p.aaa5694-aaa5694. Available at: http://www.sciencemag.org/cgi/doi/10.1126/science.aaa5694.

Bruno, R.M., 2011. Synchrony in sensation. *Current Opinion in Neurobiology*, 21(5), pp.701–708.

Carandini, M. & Heeger, D., 2012. Normalization as a canonical neural computation. *Nature*

Reviews Neuroscience, (November), pp.1–12. Available at: http://discovery.ucl.ac.uk/1332718/.

Cash, S. & Yuste, R., 1999. Linear summation of excitatory inputs by CA1 pyramidal neurons. *Neuron*, 22(2), pp.383–394.

Chance, F.S., Abbott, L.F. & Reyes, A.D., 2002. Gain modulation from background synaptic input. *Neuron*, 35(4), pp.773–782.

Cohen, J.D., Bolstad, M. & Lee, A.K., 2017. Experience-dependent shaping of hippocampal CA1 intracellular activity in novel and familiar environments. *eLife*, 6.

D'amour, J.A. & Froemke, R.C., 2015. Inhibitory and Excitatory Spike-Timing-Dependent Plasticity in the Auditory Cortex. *Neuron*, 86(2), pp.514–528. Available at: http://www.sciencedirect.com/science/article/pii/S089662731500210X.

Denève, S. & Machens, C.K., 2016. Efficient codes and balanced networks. *Nature neuroscience*, 19(3), pp.375–82. Available at: http://www.ncbi.nlm.nih.gov/pubmed/26906504.

Epsztein, J., Brecht, M. & Lee, A.K., 2011. Intracellular Determinants of Hippocampal CA1 Place and Silent Cell Activity in a Novel Environment. *Neuron*, 70(1), pp.109–120.

Froemke, R.C., 2015. Plasticity of Cortical Excitatory-Inhibitory Balance. *Annual Review of Neuroscience*, 38(1), pp.195–219. Available at: http://www.annualreviews.org/doi/10.1146/annurev-neuro-071714-034002.

Froemke, R.C., Merzenich, M.M. & Schreiner, C.E., 2007. A synaptic memory trace for cortical receptive field plasticity. *Nature*, 450(7168), pp.425–429. Available at: http://www.nature.com/doifinder/10.1038/nature06289 [Accessed March 8, 2017].

Gabernet, L. et al., 2005. Somatosensory integration controlled by dynamic thalamocortical feed-forward inhibition. *Neuron*, 48(2), pp.315–327.

Gasparini, S., 2006. State-Dependent Dendritic Computation in Hippocampal CA1 Pyramidal Neurons. *Journal of Neuroscience*, 26(7), pp.2088–2100. Available at:

http://www.jneurosci.org/cgi/doi/10.1523/JNEUROSCI.4428-05.2006.

Haider, B. et al., 2006. Neocortical Network Activity In Vivo Is Generated through a Dynamic Balance of Excitation and Inhibition. *Journal of Neuroscience*, 26(17).

Heiss, J.E. et al., 2008. Shift in the Balance between Excitation and Inhibition during Sensory Adaptation of S1 Neurons. *Journal of Neuroscience*, 28(49), pp.13320–13330. Available at: http://www.jneurosci.org/cgi/doi/10.1523/JNEUROSCI.2646-08.2008.

Hennequin, G., Agnes, E.J. & Vogels, T.P., 2017. Inhibitory Plasticity: Balance, Control, and Codependence. *Annual Review of Neuroscience*, 40(1), p.annurev-neuro-072116-031005. Available at: http://www.ncbi.nlm.nih.gov/pubmed/28598717%5Cnhttp://www.annualreviews.org/doi/10.1146/annurev-neuro-072116-031005.

Higley, M.J. & Contreras, D., 2006. Balanced Excitation and Inhibition Determine Spike Timing during Frequency Adaptation. *Journal of Neuroscience*, 26(2), pp.448–457. Available at: http://www.jneurosci.org/cgi/doi/10.1523/JNEUROSCI.3506-05.2006.

Isaacson, J.S. & Scanziani, M., 2011. How inhibition shapes cortical activity. *Neuron*, 72(2), pp.231–243. Available at: http://dx.doi.org/10.1016/j.neuron.2011.09.027.

Ishizuka, N., Cowan, W.M. & Amaral, D.G., 1995. A quantitative analysis of the dendritic organization of pyramidal cells in the rat hippocampus. *J Comp Neurol*, 362(April), pp.17–45. Available at: http://www.ncbi.nlm.nih.gov/pubmed/8576427%5Cnhttp://onlinelibrary.wiley.com/store/10.1002/cne.903620103/asset/903620103_ftp.pdf?v=1&t=hhvv55q7&s=710f922a2f06be065f4a09d53e6dde2473fd5f7c.

Ishizuka, N., Weber, J. & Amaral, D.G., 1990. Organization of intrahippocampal projections originating from CA3 pyramidal cells in the rat. *Journal of Comparative Neurology*, 295(4), pp.580–623.

Jensen, O. & Lisman, J.E., 2000. Position Reconstruction From an Ensemble of Hippocampal

Place Cells: Contribution of Theta Phase Coding. *Journal of Neurophysiology*, 83(5), pp.2602–2609. Available at: http://jn.physiology.org/content/83/5/2602%5Cnhttp://jn.physiology.org/content/83/5/2602.full.pdf%5Cnhttp://jn.physiology.org/content/83/5/2602.long.

Klyachko, V.A. et al., 2006. Excitatory and Feed-Forward Inhibitory Hippocampal Synapses Work Synergistically as an Adaptive Filter of Natural Spike Trains I. Segev, ed. *PLoS Biology*, 4(7), p.e207. Available at: http://dx.plos.org/10.1371/journal.pbio.0040207 [Accessed January 8, 2017].

Kremkow, J., Aertsen, A. & Kumar, A., 2010. Gating of Signal Propagation in Spiking Neural Networks by Balanced and Correlated Excitation and Inhibition. *Journal of Neuroscience*, 30(47), pp.15760–15768. Available at: http://www.jneurosci.org/cgi/doi/10.1523/JNEUROSCI.3874-10.2010.

Magee, J.C. & Cook, E.P., 2000. Somatic EPSP amplitude is independent of synapse location in hippocampal pyramidal neurons. *Nature neuroscience*, 3(9), pp.895–903.

Murthy, V.N., Sejnowski, T.J. & Stevens, C.F., 1997. Heterogeneous release properties of visualized individual hippocampal synapses. *Neuron*, 18, pp.599–612.

Okun, M. & Lampl, I., 2008. Instantaneous correlation of excitation and inhibition during ongoing and sensory-evoked activities. *Nature neuroscience*, 11(5), pp.535–7. Available at: http://www.ncbi.nlm.nih.gov/pubmed/18376400 [Accessed June 1, 2017].

Panzeri, S. et al., 2001. The role of spike timing in the coding of stimulus location in rat somatosensory cortex. *Neuron*, 29(3), pp.769–777.

Poirazi, P., Brannon, T. & Mel, B.W., 2003. Arithmetic of Subthreshold Synaptic Summation in a Model CA1 Pyramidal Cell. *Neuron*, 37(6), pp.977–987. Available at: http://www.sciencedirect.com/science/article/pii/S089662730300148X [Accessed September 3, 2015].

Pouille, F. et al., 2009. Input normalization by global feedforward inhibition expands cortical

dynamic range. *Nature neuroscience*, 12(12), pp.1577–85. Available at: http://www.ncbi.nlm.nih.gov/pubmed/19881502.

Pouille, F. & Scanziani, M., 2001. Enforcement of temporal fidelity in pyramidal cells by feed-forward somatic inhibition. *Science*, 293(5532), pp.325–331. Available at: http://www.sciencemag.org/cgi/doi/10.1126/science.1060342.

Reynolds, J.H. & Heeger, D.J., 2009. The Normalization Model of Attention. *Neuron*, 61(2), pp.168–185.

Shadlen, M.N. & Newsome, W.T., 1998. The variable discharge of cortical neurons: implications for connectivity, computation, and information coding. *The Journal of neuroscience : the official journal of the Society for Neuroscience*, 18(10), pp.3870–96. Available at: http://www.ncbi.nlm.nih.gov/pubmed/9570816.

Shannon, C.E., 1948. A Mathematical Theory of Communication. *Bell System Technical Journal*, 27(3), pp.379–423.

Sherman, S.M. & Guillery, R.W., 1998. On the actions that one nerve cell can have on another: Distinguishing “drivers” from “modulators.” *Proceedings of the National Academy of Sciences*, 95(12), pp.7121–7126. Available at: http://www.pnas.org/cgi/doi/10.1073/pnas.95.12.7121.

Shu, Y. et al., 2003. Barrages of Synaptic Activity Control the Gain and Sensitivity of Cortical Neurons. *Journal of Neuroscience*, 23(32).

Silver, R.A., 2010. Neuronal arithmetic. , 11(June).

Thompson, L.T. & Best, P.J., 1989. Place cells and silent cells in the hippocampus of freely-behaving rats. *The Journal of neuroscience : the official journal of the Society for Neuroscience*, 9(7), pp.2382–90. Available at: http://www.ncbi.nlm.nih.gov/pubmed/2746333.

Tsodyks, M. V. & Markram, H., 1997. The neural code between neocortical pyramidal neurons depends on neurotransmitter release probability. *Proceedings of the National Academy of*

Sciences, 94(2), pp.719–723. Available at: http://www.pnas.org/cgi/doi/10.1073/pnas.94.2.719.

Vogels, T.P. et al., 2011. Inhibitory plasticity balances excitation and inhibition in sensory pathways and memory networks. *Science (New York, N.Y.)*, 334(6062), pp.1569–73. Available at: http://science.sciencemag.org/content/334/6062/1569.abstract.

Vogels, T.P. & Abbott, L.F., 2009. Gating multiple signals through detailed balance of excitation and inhibition in spiking networks. *Nature neuroscience*, 12(4), pp.483–91. Available at: http://www.ncbi.nlm.nih.gov/pubmed/19305402.

van Vreeswijk, C. & Sompolinsky, H., 1996. Chaos in neuronal networks with balanced excitatory and inhibitory activity. *Science (New York, N.Y.)*, 274(5293), pp.1724–6. Available at: http://www.ncbi.nlm.nih.gov/pubmed/8939866 [Accessed June 1, 2017].

Wehr, M. & Zador, A.M., 2003a. Balanced inhibition underlies tuning and sharpens spike timing in auditory cortex. *Nature*, 426(6965), pp.442–446. Available at: http://www.nature.com/doifinder/10.1038/nature02116 [Accessed May 2, 2017].

Wehr, M. & Zador, A.M., 2003b. Balanced inhibition underlies tuning and sharpens spike timing in auditory cortex. *Nature*, 426(6965), pp.442–446. Available at: http://www.ncbi.nlm.nih.gov/pubmed/14647382.

Wilent, W.B. & Contreras, D., 2005. Dynamics of excitation and inhibition underlying stimulus selectivity in rat somatosensory cortex. *Nature Neuroscience*, 8(10), pp.1364–1370. Available at: http://www.nature.com/doifinder/10.1038/nn1545 [Accessed June 26, 2017].

Xue, M., Atallah, B. V. & Scanziani, M., 2014. Equalizing excitation–inhibition ratios across visual cortical neurons. *Nature*, 511(7511), pp.596–600. Available at: http://www.nature.com/doifinder/10.1038/nature13321 [Accessed January 19, 2017].

Yizhar, O. et al., 2011. Neocortical excitation/inhibition balance in information processing and social dysfunction. *Nature*, 477(7363), pp.171–178. Available at: http://www.nature.com/doifinder/10.1038/nature10360.

Zhang, L.I. et al., 2003. Topography and synaptic shaping of direction selectivity in primary auditory cortex. *Nature*, 424(6945), pp.201–205. Available at: http://www.nature.com/doifinder/10.1038/nature01796.

Zhou, M. et al., 2014. Scaling down of balanced excitation and inhibition by active behavioral states in auditory cortex. *Nature Neuroscience*, 17(6), pp.841–850. Available at: http://www.nature.com/doifinder/10.1038/nn.3701.